# Analysis of dark matter profiles in the halos of spiral galaxies

Ye. Kurmanov[1,2,3] , K. Boshkayev[1,2]* , T. Konysbayev[1,2] , M. Muccino[1,4] ,

A. Urazalina[1,2] , G. Ikhsan[1] , N. Saiyp[2] , G. Rabigulova[2] ,

M. Karlinova[2] , G. Suliyeva[1,2] , A. Taukenova[2] and N. Beissen[2]

[1]National Nanotechnology Laboratory of Open Type, Almaty, Kazakhstan
[2]Al-Farabi Kazakh National University, Almaty, Kazakhstan
[3]International Engineering Technological University, Almaty, Kazakhstan
[4]Istituto Nazionale di Fisica Nucleare, Laboratori Nazionali di Frascati, Frascati, Italy
*e-mail: kuantay@mail.ru
*(Received September 5, 2023; received in revised form October 3, 2023; accepted October 10, 2023)*

The dark matter content in the spiral galaxies with low surface brightness U5750, U11454, U11819, and U11648 is analyzed by utilizing well-established density profiles from existing literature. These profiles include the Beta, Brownstein, Burkert, exponential sphere, pseudo-isothermal, and Persic profiles. For simplicity, without accounting for the intricate structural complexities in the aforementioned galaxies, we assume that the dark matter distribution is spherically symmetric. For each density profile, the data points from the rotation curves of the galaxies under consideration are fitted. We infer model-free quantities, such as the central (characteristic) density and scale radius, from the rotation curves employing Markov Chain Monte Carlo analyses. This enables us to estimate the total dark matter mass in the galactic halos. We exploit the Bayesian Information Criterion to determine the best-fit profile. Additionally, we adopt the nonlinear least squares approach of Levenberg-Marquardt for comparison and completeness. Through our statistical analysis, we offer a physical interpretation behind the selection of specific profiles, based on the insights obtained from the analyses.

## 1 Introduction

Numerous astrophysical and cosmological phenomena can be consistently explained by the presence of dark matter (DM). These phenomena encompass rotation curves (RCs) of stars in galaxies, cosmic microwave background anisotropies, the magnitude-redshift relation of type Ia supernovae, Big Bang Nucleosynthesis, gravitational lensing, the formation of the Universe's large-scale structure, baryonic oscillations, and effects observed during galaxy cluster collisions, among others [1, 2].

Recent cosmological surveys have indicated that DM accounts for 26.8% of the Universe's overall energy budget [3]. All information about DM is indirectly obtained by astronomers and astrophysicists through the study of galaxies' RCs and the effects of gravitational lensing. RCs serve various purposes, including the investigation of

galaxies' kinematics, the inference of their evolutionary histories, the determination of the role played by interactions, and the correlation of deviations from the expected RC form with the amount and distribution of DM, among others. The investigation of galaxy RCs began with nearby galaxies like M31. In Ref. [4], the authors examined the RCs of M31 and observed that the galaxy's outer regions rotated at nearly constant speeds. Additionally, radio observations of HI gas revealed almost flat RCs in the M31 [5] and M33 [6] galaxies.

Over the past few years, astrophysicists have directed significant attention toward the RCs of galaxies with low surface brightness (LSB) and the constraints they impose on cosmological theories [7-10]. An LSB galaxy is typically characterized as a disk galaxy with an estimated central disk surface brightness of approximately brightness ~ 1 mag arcsec$^{-2}$ [7]. These LSB galaxies are dominated by

DM, making an investigation of their RCs a valuable source of information regarding the characteristics and distribution of DM [11-13].

In this article, we examine the DM distribution in the LSB galaxies U5750, U11454, U11819, and U11648, using recent RC data and employing various phenomenological density profiles, including Burkert, Beta, exponential sphere, Brownstein, pseudo-isothermal (ISO), and Persic. The RC data points for these galaxies are provided in Ref. [9, 10]. We employ the Markov Chain Monte Carlo (MCMC) statistical analysis method to determine the best-fit models. In order to establish the priors for the MCMC analyses, we use the nonlinear least squares approach by Levenberg-Marquardt, which allows us to determine the minimal value of $\chi^2$. Finally, we compute the DM mass within the halos of these galaxies.

This article is structured as follows: Section 2 outlines the various empirical DM profiles. Section 3 presents the fitting methods for the RCs data of the LSB galaxies U11454, U11648, U11819 and U5750, along with the major numerical results. Finally, Section 4 summarizes our conclusions.

## 2 Phenomenological profiles of dark matter

The dynamic evolution of galaxies as well as the evolution of the universe depend on the distribution of DM in galaxies. In general, the distribution of DM is not uneven inside galaxies, it piles up at their center, and decreases at the edges. Utilizing numerical simulation methods of star motion in galaxies can provide the relevant DM distribution function or profile. Several DM profiles have been postulated in the literature. For instance, in Ref. [14], the author developed a phenomenological profile to describe dwarf spiral galaxies' RCs. In Ref. [15], the authors demonstrated that the ISO profile might match a broad sample of galaxy RCs. According to Ref. [16, 17], the RCs of LSB galaxies exhibit excellent agreement with the core-modified profile with a constant central density.

Here, we use popular DM density profiles in this work, including the Persic, exponential sphere, Burkert, ISO, Brownstein, and Beta. Apart from the Persic profile, which depends upon $\beta_0$ and $a$, the other density profiles used in this study are specified by two parameters: $r_0$ (scale radius) and $\rho_0$ (central density).

As a result, we use the following models:
The Beta profile with $\beta = 1$ [16, 18]:

$$\rho_{Beta}(r) = \frac{\rho_0}{\left(1+x^2\right)^{3/2}}. \tag{1}$$

Brownstein profile [16, 17]:

$$\rho_{Bro}(r) = \frac{\rho_0}{1+x^3}. \tag{2}$$

Burkert profile [14]:

$$\rho_{Bur}(r) = \frac{\rho_0}{\left(1+x\right)\left(1+x^2\right)}. \tag{3}$$

Exponential sphere [16]:

$$\rho_{Exp}(r) = \rho_0 e^{-x}. \tag{4}$$

The ISO profile [15]:

$$\rho_{Iso}(r) = \frac{\rho_0}{1+x^2}, \tag{5}$$

where $x = x(r) = r/r_0$, $r$ is the radial coordinate. All density profiles depend on the two constants $\rho_0$ and $r_0$.

We consider the profile of velocity suggested by Persic et al. [10, 19] that was proposed by analyzing 1023 galaxies and is represented as:

$$\beta^2 = \beta_0^2 \frac{x^2}{x^2 + a^2}, \tag{6}$$

where $\beta_0$ and $a$ are the parameters of the model. Here, $\beta_0$ represents the terminal velocity's ratio to the speed of light, while the second, denoted by $a$, specifies how quickly the velocity achieves a terminal value.

## 3 Statistical methods and numerical outcomes

Here by adopting the density profiles for halos, we fit the RC data, using MCMC procedure and define the models' free parameters.

We show that the kinematics of the entire spiral galaxies, which include U11648, U5750, U11454, and U11819 can be effectively described by the

density profiles of DM halos. We achieve this by evaluating various profiles for these galaxies. To be clear, taking into account the gas content in the disk and bulge of the galaxy is critical for describing the RCs. The RC makes it possible to calculate how the mass of a galaxy is distributed over radial distances. But all galaxy components must be duly taken into account, as described in [20]. They nevertheless make only a small amount of contribution to the DM mass in the halo.

Furthermore, the inner regions of galaxies U11819, U5750, U11454, and U11648 are not thoroughly described in the literature. Taking this fact into account, for simplicity, one can focus only on the halo and adopt

$$v_{tot}^2 \simeq v_{profile}^2, \tag{7}$$

where $v_{profile}$ is the velocity profile of the DM halo.

As a result, $v_{profile}$ is defined as

$$v_{profile} = v(r) = \sqrt{\frac{GM(r)}{r}}, \tag{8}$$

By integrating the mass balance formula, we get the DM mass profile $M(r)$ in Eq. (8).

$$M(r) = \int_0^r 4\pi r^2 \rho(r) dr, \tag{9}$$

where $\rho(r)$ is the DM density profile given by Eqs. (1 − 5).

To further determine the $\chi^2$ function's minimum, we use the nonlinear least squares Levenberg-Marquardt method [21, 22]. The $\chi^2$ function is defined as

$$\chi^2 = \sum_{i=1}^N \left[ \frac{v_i^{obs} - v(\rho_0, r_0, r)}{\sigma_{v,i}^{obs}} \right]^2, \tag{10}$$

where $v_i^{obs}$ and $\sigma_{v,i}^{obs}$ are the RCs and their related errors (see Fig. 1) and $N$ is the data point number of the galaxies U11454, U11648, U5750 and U11819, respectively.

In this work, by employing the Bayesian Information Criterion (BIC) [23], we evaluate six selected density profiles and determine the best-fit model from them. BIC is a model selection criteria designed to tackle the problem of overfitting when the amount of parameters in the function of the fitting is increased. The BIC is defined by:

$$\text{BIC} = \chi^2 + k \ln N, \tag{11}$$

where, $k$ stands for the quantity of model parameters. For our selected six models, $k = 2$. Density profiles with the smallest BIC is preferable [24].

The reference model is the one with the smallest BIC, say $\text{BIC}_0$, so $\Delta\text{BIC} = \text{BIC-BIC}_0$

When comparing models, the evidence against a model or, equivalently, in favor of the reference model can be summarized as follows:

- $\Delta\text{BIC}$ [0,3], weak evidence;
- $\Delta\text{BIC}$ (3,6], mild evidence;
- $\Delta\text{BIC} > 6$, strong evidence.

So, the best model will be the one(s) with lowest BIC (the situation has to be analyzed case by case). Naturally, the reference model has always $\Delta\text{BIC}=0$.

The probability distribution of the model set, in the parameter space, is generated using a Bayesian method known as MCMC.

We employ the Metropolis-Hastings algorithm, searching for best-fit parameters that maximize the log-likelihood

$$L = -\frac{1}{2} \left[ \chi^2 + \sum_{i=1}^N \ln\left(\sqrt{2\pi}\sigma_{v,i}^{obs}\right) \right], \tag{12}$$

Further, the *Wolfram Mathematica* code from [25] is modified and adapted to the case of RCs data. We consider the different priors over the coefficients: $\rho_0$ and $r_0$.

## 4 Results and Discussion

In Refs. [26-28], some of us investigated the RCs of galaxies, specifically focusing on U5750, U11454, and ESO140040. In these studies, we considered well-established density profiles. For instance, in the case of the U5750 galaxy, the Einasto profile demonstrated the lowest BIC, while the ISO profile exhibited the highest BIC [26]. However, in the

current study, we opted not to utilize the Einasto profile due to its poor performance with MCMC analysis. In our investigation of the U5750 galaxy, the Brownstein profile yielded the most favorable BIC, with the ISO profile delivering less favorable results, consistent with the findings in [26].
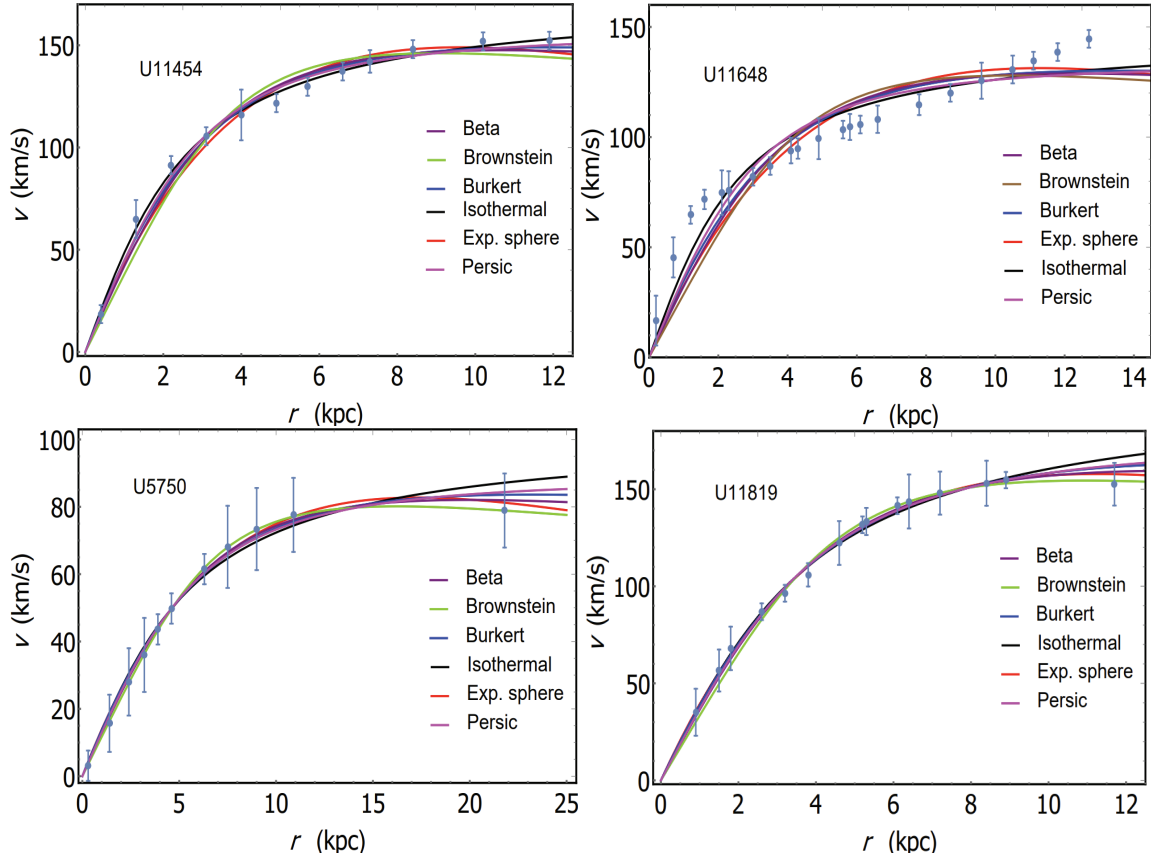


**Figure 1** – RCs of galaxies and fitted profiles

Figure 1 depicts the RCs of the galaxies U11819, U5750, U11454, and U11648, as well as the theoretical curves for various profiles employed here. In this figure, we have concentrated on the galaxies halo region. The observational data, shown as thick blue dots with their corresponding error bars, are contrasted with the fitted Beta (magenta), Brownstein (green), Burkert (blue), exponential sphere (red), ISO (black), and Persic (purple) profiles, represented by solid curves.

In Ref. [27], it was observed that the ISO profile provided an excellent description of the observational data for the U11454 galaxy, while the Brownstein profile proved less effective in modeling the rotation curves for this galaxy. Our results for the U11454 galaxy align well with those presented in Ref. [27].

Moreover, in Ref. [10], the authors introduced a model for galactic halos, characterizing DM as a fluid with non-zero pressure. By employing observational data from the rotation curves of galaxies, they derived the equation of state for DM. Additionally, they demonstrated that the free parameters in the equation of state were determined by fitting the observed velocities in the rotation curves with the velocities predicted by each DM profile.
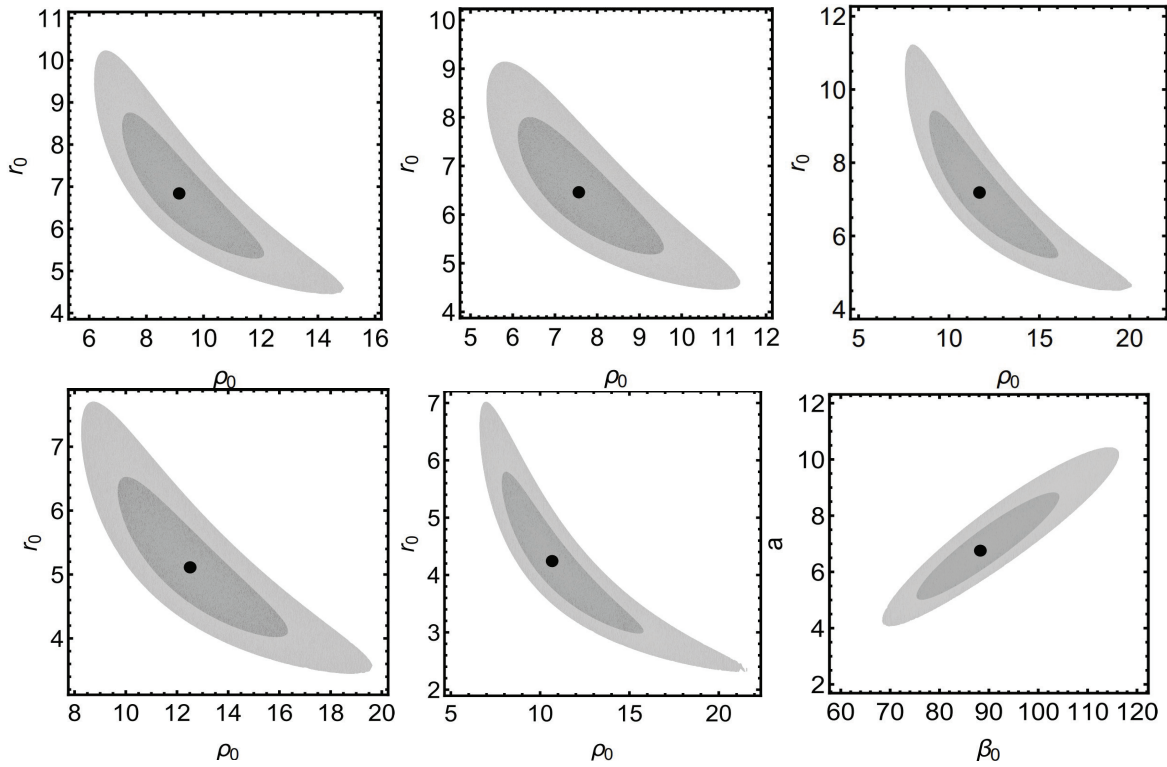
**Figure 2** – Galaxy U5750. Contours plots of the best-fit parameters (black dots) and the associated
$1-\sigma$ (dark gray) and $2-\sigma$ (light gray) confidence regions of the sources listed in Table 1. Top panel left: Beta, middle:
Brownstein, right: Burkert. Bottom panel left: Exp. sphere, middle: Isothermal, right: Persic



**Figure 3** – Galaxy U11454. Contours plots of the best-fit parameters (black dots) and the associated
$1-\sigma$ (dark gray) and $2-\sigma$ (light gray) confidence regions of the sources listed in Table 2. Top panel left: Beta, middle:
Brownstein, right: Burkert. Bottom panel left: Exp. sphere, middle: Isothermal, right: Persic
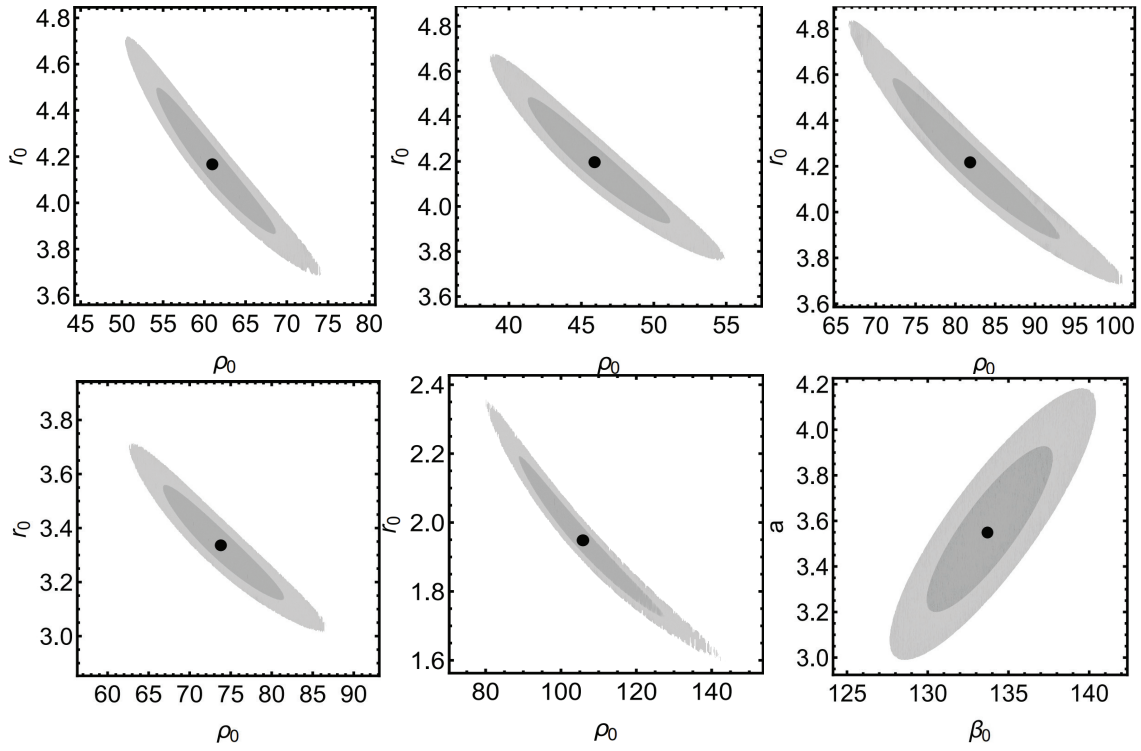
**Figure 4** – Galaxy U11648. Contours plots of the best-fit parameters (black dots) and the associated
1−$\sigma$ (dark gray) and 2−$\sigma$ (light gray) confidence regions of the sources listed in Table 3. Top panel left: Beta, middle:
Brownstein, right: Burkert. Bottom panel left: Exp. sphere, middle: Isothermal, right: Persic
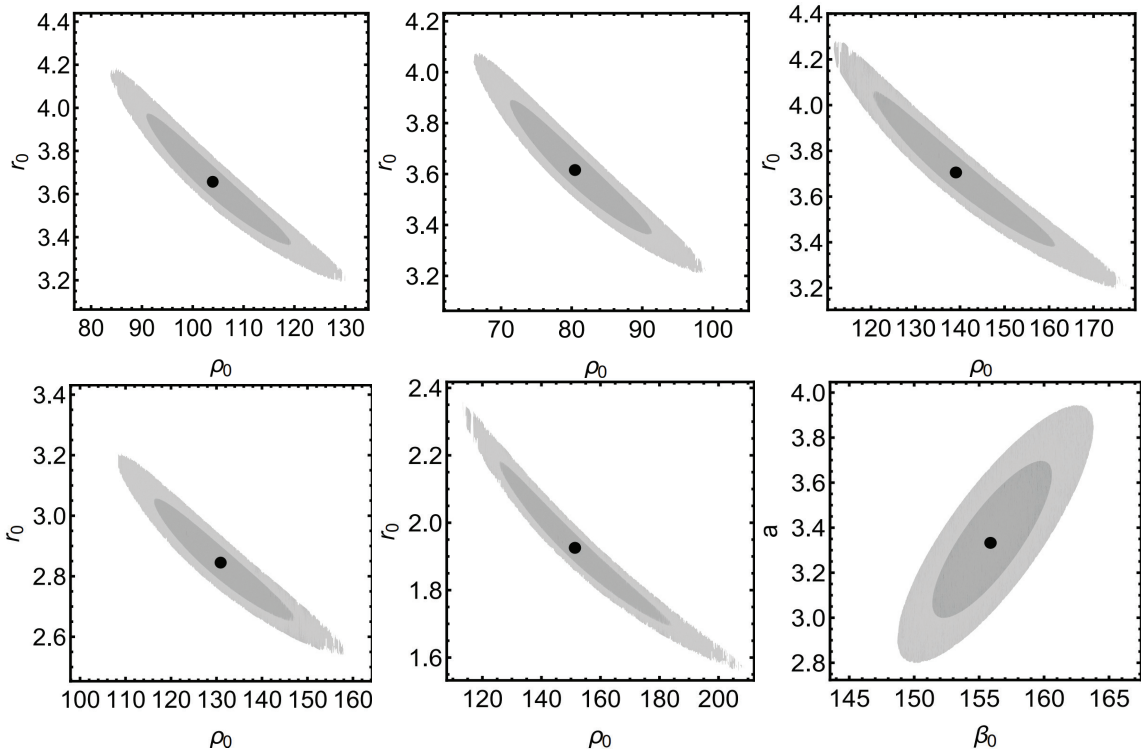


**Figure 5** – Galaxy U11819. Contours plots of the best-fit parameters (black dots) and the associated
1−$\sigma$ (dark gray) and 2−$\sigma$ (light gray) confidence regions of the sources listed in Table 4. Top panel left: Beta, middle:
Brownstein, right: Burkert. Bottom panel left: Exp. sphere, middle: Isothermal, right: Persic
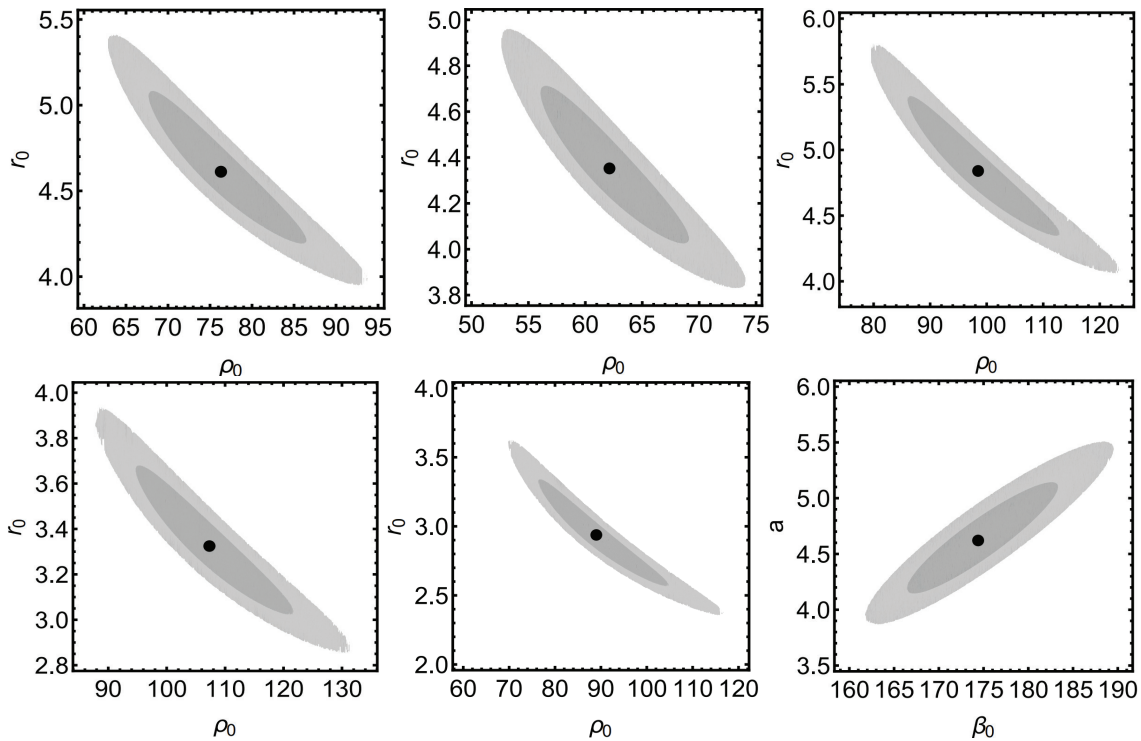
In Figs. 2, 3, 4 and 5 we display the contour plots of the best-fit parameters for the galaxies U11819, U5750, U11454, and U11648 using different models, respectively.

In Ref. [29], the authors considered two sets of galaxy rotation curves based on the availability of photometric data. For LSB galaxies, where DM predominates, high-resolution observational data from the rotation curves of 18 LSB galaxies were utilized.

Ref. [30] delved into the impact of gas pressure generated by electrons and positrons resulting from DM annihilation in LSB galaxies. The authors proposed that electrons and positrons are products of DM annihilation and can dissipate their energy through various loss processes into photons and the interstellar medium within galaxies.

Various effects of dark matter, including those associated with isotropic, anisotropic, and tangential pressures on the accretion disk luminosity around astrophysical black holes, have been examined in [31-33]. Additionally, other significant attributes of dark matter, such as its influence on the motion of test particles, have been investigated in the contexts of both Newtonian gravity and general relativity, as discussed in [34-36].

Furthermore, the results obtained with the MCMC for U5750 galaxy are presented in Table 1 and compared with the ones inferred using the *NonlinearModelFit* fitting procedure in Table A1 (see Appendix). In all tables we provided the $\rho_0$, $r_0$, $M_{vir}$, $r_{vir}$ virial radius specified as the radius at which the density is equal to the universe's critical density times 200, masses in terms of $M_\odot$, BIC and $\chi^2$ values for each profile. Tables 1 and A1 show that the difference in $\rho_0$, $r_0$, $M_{vir}$, $r_{vir}$, masses in terms of $M_\odot$, BIC and $\chi^2$ values is not significant. The only difference is in the error bars.

Table 1 shows that the $\chi^2$ value for the galaxy U5750 is lowest for the Brownstein profile and highest for the ISO profile.

**Table 1** – The parameters of the best-fit model for galaxy U5750 with MCMC

| Profiles | $\rho_0 \pm \sigma_{\rho_0}$, $\left(10^{-3}\frac{M_\odot}{pc^3}\right)$ | $r_0 \pm \sigma_{r_0}$, $(\text{kpc})$ | $r_{vir}$, $(\text{kpc})$ | $M_{vir}$, $(10^{10}M_\odot)$ | $M \pm \sigma_M{}^a$, $(10^{10}M_\odot)$ | $M \pm \sigma_M{}^b$, $(10^9 M_\odot)$ | $\Delta$BIC | $\chi^2$ |
|---|---|---|---|---|---|---|---|---|
| Beta | $9.16^{+2.95(+5.72)}_{-2.01(-3.00)}$ | $6.85^{+1.91(+3.37)}_{-1.55(-2.40)}$ | 46.97 | 6.04 | $3.40 \pm 0.22$ | $6.44 \pm 0.79$ | 0.25 | 0.28 |
| Brown. | $7.57^{+2.00(+3.81)}_{-1.45(-2.20)}$ | $6.47^{+1.53(+2.66)}_{-1.29(-2.00)}$ | 42.05 | 4.83 | $3.15 \pm 0.18$ | $5.96 \pm 0.62$ | 0 | 0.03 |
| Burkert | $11.72^{+4.31(+8.28)}_{-2.82(-4.16)}$ | $7.17^{+2.25(+4.05)}_{-1.78(-2.67)}$ | 51.32 | 7.18 | $3.54 \pm 0.25$ | $6.90 \pm 0.95$ | 0.67 | 0.70 |
| Exp. sph. | $12.50^{+3.83(+7.12)}_{-2.82(-4.20)}$ | $5.11^{+1.42(+2.60)}_{-1.08(-1.66)}$ | 31.24 | 3.94 | $3.34 \pm 0.10$ | $3.36 \pm 0.11$ | 0.43 | 0.47 |
| ISO | $10.69^{+5.07(+10.89)}_{-2.84(-4.08)}$ | $4.24^{+1.56(+2.76)}_{-1.26(-1.93)}$ | 83.42 | 18.56 | $3.85 \pm 0.18$ | $2.19 \pm 0.10$ | 1.34 | 1.37 |
| Persic | — | — | — | — | 3.44 | — | 0.61 | 0.64 |

Note that for the Persic profile $\beta_0 = 88.31^{+15.96(+28.05)}_{-12.92(-19.92)}$, and $a = 0.72^{+1.07(+1.08)}_{-0.46(-0.57)}$.

[a]The mass of DM computed for $r$ employing the last data point in the halo.

[b]The mass of DM estimated employing the scale radius $r_0$.

The values BIC = {5.44, 4.83, 6.17, 5.26, 5.50, 5.08} are for the Persic, Brownstein, ISO, Exp.sph., Burkert and Beta. We denote $\Delta$BIC = BIC-BIC$_0$, with BIC$_0$=4.83 (the reference value) for the Brownstein profile.

For the galaxy U11454, the $\chi^2$ value is the highest for the Brownstein profile of all the profiles taken into consideration, while for the ISO is the lowest. The same applies to the $\Delta$BIC (see Table 2).

**Table 2** – The parameters of the best-fit model for galaxy U11454 with MCMC.

| Profiles | $\rho_0 \pm \sigma_{\rho_0}$, $\left(10^{-3}\frac{M_\odot}{pc^3}\right)$ | $r_0 \pm \sigma_{r_0}$, (kpc) | $r_{vir}$, (kpc) | $M_{vir}$, $(10^{11}M_\odot)$ | $M \pm \sigma_M{}^a$, $(10^{10}M_\odot)$ | $M \pm \sigma_M{}^b$, $(10^{10}M_\odot)$ | $\Delta$BIC | $\chi^2$ |
|---|---|---|---|---|---|---|---|---|
| Beta | $103.98^{+15.36(+26.60)}_{-13.14(-20.48)}$ | $3.65^{+0.32(+0.53)}_{-0.29(-0.46)}$ | 56.82 | 1.56 | $6.00 \pm 1.40$ | $1.11 \pm 0.44$ | 10.97 | 14.79 |
| Brown. | $80.59^{+10.72(+18.35)}_{-9.33(-14.64)}$ | $3.61^{+0.28(+0.46)}_{-0.25(-0.41)}$ | 51.74 | 1.27 | $5.75 \pm 1.22$ | $1.11 \pm 0.38$ | 24.32 | 28.14 |
| Burkert | $139.04^{+22.36(+38.53)}_{-18.81(-27.39)}$ | $3.70^{+0.36(+0.57)}_{-0.32(-0.52)}$ | 62.29 | 1.86 | $6.14 \pm 1.54$ | $1.13 \pm 0.49$ | 5.99 | 9.81 |
| Exp. sph. | $130.83^{+16.51(+27.44)}_{-14.61(-23.07)}$ | $2.84^{+0.21(+0.36)}_{-0.19(-0.30)}$ | 24.07 | 0.75 | $5.95 \pm 1.27$ | $0.61 \pm 0.21$ | 13.07 | 16.89 |
| ISO | $151.26^{+33.04(+59.53)}_{-25.78(-39.31)}$ | $1.93^{+0.26(+0.44)}_{-0.23(-0.37)}$ | 142.80 | 9.86 | $6.47 \pm 2.06$ | $0.29 \pm 0.17$ | 0 | 3.82 |
| Persic | — | — | — | — | 5.95 | — | 4.25 | 8.07 |

For the Persic profile $\beta_0 = 155.86^{+4.74(+7.95)}_{-4.45(-7.16)}$, and $a = 3.33^{+0.36(+0.61)}_{-0.33(-0.53)}$.

For the U11454 the Beta, Burkert, Exp. sph., Brownstein, ISO and Persic density profiles are each represented by the values BIC = {19.76, 14.78, 21.86, 33.11, 8.79, 13.04}, respectively. $BIC_0$=8.79 (ISO density profile).

The $\chi^2$ value for the U11648 galaxy is least for the ISO profile and greatest for the Brownstein profile, as shown in Table 3. The values BIC = {112.59, 115.17, 131.23, 80.66, 183.40, 138.74} are listed for the Persic, Burkert, Exp. sph., ISO, Brownstein, and Beta. We find that $BIC_0$=80.66 is for the ISO.

**Table 3** – The parameters of the best-fit model for galaxy U11648 with MCMC.

| Profiles | $\rho_0 \pm \sigma_{\rho_0}$, $\left(10^{-3}\frac{M_\odot}{pc^3}\right)$ | $r_0 \pm \sigma_{r_0}$, (kpc) | $r_{vir}$, (kpc) | $M_{vir}$, $(10^{11}M_\odot)$ | $M \pm \sigma_M{}^a$, $(10^{10}M_\odot)$ | $M \pm \sigma_M{}^b$, $(10^9 M_\odot)$ | $\Delta$BIC | $\chi^2$ |
|---|---|---|---|---|---|---|---|---|
| Beta | $60.90^{+7.79(+13.44)}_{-6.72(-10.56)}$ | $4.17^{+0.33(+0.55)}_{-0.30(-0.49)}$ | 54.18 | 1.25 | $4.90 \pm 1.00$ | $9.67 \pm 3.47$ | 58.08 | 132.56 |
| Brown. | $45.88^{+5.24(+9.00)}_{-4.60(-7.20)}$ | $4.20^{+0.29(+0.48)}_{-0.27(-0.44)}$ | 49.75 | 1.05 | $4.77 \pm 0.89$ | $9.84 \pm 3.08$ | 102.74 | 177.22 |
| Burkert | $81.83^{+11.32(+19.50)}_{-9.74(-15.18)}$ | $4.22^{+0.37(+0.62)}_{-0.34(-0.54)}$ | 59.17 | 1.49 | $4.99 \pm 1.10$ | $9.81 \pm 3.88$ | 34.51 | 108.99 |
| Exp. sph. | $73.81^{+7.72(+13.03)}_{-7.07(-11.21)}$ | $3.33^{+0.22(+0.38)}_{-0.20(-0.32)}$ | 26.33 | 0.68 | $5.04 \pm 0.90$ | $5.53 \pm 1.68$ | 50.57 | 125.05 |
| ISO | $105.89^{+21.70(+38.09)}_{-17.17(-26.24)}$ | $1.95^{+0.25(+0.41)}_{-0.22(-0.35)}$ | 120.85 | 5.95 | $5.02 \pm 1.51$ | $2.11 \pm 1.21$ | 0 | 74.78 |
| Persic | — | — | — | — | 4.68 | — | 31.63 | 106.41 |

For the Persic profile $\beta_0 = 133.72^{+6.72(+4.01)}_{-6.05(-3.79)}$, and $a = 3.55^{+0.63(+0.38)}_{-0.56(-0.35)}$.

According to Table 4, for galaxy U11819 the BIC and $\chi^2$ values are lowest for the Exp sph. profile and highest for the ISO profile. The values do not significantly differ from one another (see Table A4 in Appendix for comparison).

**Table 4** – The parameters of the best-fit model for galaxy U11819 with MCMC

| Profiles | $\rho_0 \pm \sigma_{\rho_0}$, $\left(10^{-3}\frac{M_\odot}{pc^3}\right)$ | $r_0 \pm \sigma_{r_0}$, $(kpc)$ | $r_{vir}$, $(kpc)$ | $M_{vir}$, $(10^{11}M_\odot)$ | $M \pm \sigma_M{}^a$, $(10^{10}M_\odot)$ | $M \pm \sigma_M{}^b$, $(10^{10}M_\odot)$ | $\Delta$BIC | $\chi^2$ |
|---|---|---|---|---|---|---|---|---|
| Beta | $76.33^{+10.14(+17.53)}_{-8.64(-13.48)}$ | $4.61^{+0.47(+0.80)}_{-0.42(-0.67)}$ | 64.66 | 2.20 | $6.88 \pm 0.91$ | $1.64 \pm 0.22$ | 0.56 | 2.21 |
| Brown. | $62.16^{+6.95(+11.93)}_{-6.10(-9.57)}$ | $4.35^{+0.36(+0.61)}_{-0.33(-0.52)}$ | 57.11 | 1.66 | $6.48 \pm 1.31$ | $1.49 \pm 0.55$ | 1.8 | 3.45 |
| Burkert | $98.38^{+14.54(+25.28)}_{-12.39(-19.24)}$ | $4.84^{+0.57(+0.97)}_{-0.49(-0.78)}$ | 72.34 | 2.78 | $7.09 \pm 1.83$ | $1.78 \pm 0.93$ | 0.8 | 2.45 |
| Exp. sph. | $107.38^{+14.32(+24.25}_{-12.68(-19.60)}$ | $3.32^{+0.36(+0.61)}_{-0.20(-0.47)}$ | 27.50 | 0.98 | $6.77 \pm 1.74$ | $0.80 \pm 0.38$ | 0 | 1.65 |
| ISO | $88.89^{+15.91(+28.37)}_{-12.54(-19.30)}$ | $2.93^{+0.41(+0.70)}_{-0.37(-0.58)}$ | 166.70 | 15.58 | $7.51 \pm 2.13$ | $0.60 \pm 0.37$ | 2.46 | 4.11 |
| Persic | — | — | — | — | 6.84 | — | 1.14 | 2.79 |

Note that for the Persic profile $\beta_0 = 174.46^{+8.85(+15.10)}_{-7.98(-12.68)}$, and $a = 4.62^{+0.52(+0.89)}_{-0.47(-0.75)}$.

The values $\text{BIC} \equiv \{9.53,\ 7.87,\ 7.07,\ 8.87,\ 7.63,\ 8.21\}$ are for the ISO, Burkert, Exp. sph., Brownstein, Beta and Persic. The $\text{BIC}_0 = 7.07$ is for the Exp. sph.

## 5 Conclusion and Perspectives

In this work, we examined the RC data of the LSB galaxies U11819, U5750, U11454, and U11648. For these galaxies, we assumed a spherically symmetric distribution of DM. We used the RCs of these galaxies to compute the free parameters of the profiles under consideration using the least squares method. To facilitate our analysis, we chose established density profiles of DM from the literature. We also included the Exp. sphere density profile for comparative purposes, as it is commonly used to investigate the inner regions of galaxies [20].

As a consequence of our investigation, it is clear that the ISO, Exp. sph., and Brownstein profiles provide a better fit compared to the Persic, Beta, and Burkert profiles for the galaxies under consideration, as evidenced by their smaller BICs. In general, all the models employed in this study yielded favorable outcomes; however, not all data points were aligned with the theoretical curves. These discrepancies could stem from our simplified treatment that did not account for the galaxies' complex structures and baryonic components.

Furthermore, we estimated the $r_{vir}$ and $M_{vir}$. We utilized the condition where the density is 200 times the critical density of the Universe

$\rho_{crit} = 9.31 \times 10^{-30}$ g/cm$^3$ [37]. It was revealed that the virial mass is greater than the other masses calculated using the scale radius or the last data point in the RCs.

As one may notice, there is no universal model of DM capable of providing the best fit for all galaxy RCs. Among the profiles considered for various galaxies in this study, the best fits are consistently achieved with different profiles each time. For instance, according to MCMC analyses the Brownstein profile is the best-fit model for galaxy U5750, the ISO is the best-fit model for galaxies U11454 and U11648, and the Exp. sph. profile is the best-fit model for galaxy U11819. This observation highlights the potential to explore alternative models or propose novel ones that could serve as universals, should such a possibility exist.

Further extensions of this work can encompass the inclusion of contributions from gas within the galactic bulge and disk, while considering the galaxy's composite structure [38-39]. Moreover, rather than beginning with assumptions, an intriguing approach would involve utilizing a back-scattering method to derive the most suitable profile from the data [40-41]. Additionally, investigating the RCs within the framework of fermionic [42-45] and bosonic [46-48] models for DM, alongside exploring the impacts of modified and extended theories of gravity [49-50], would add further depth to the analysis. These aspects will be considered in our forthcoming research.

**Appendix**

In the appendix, we present our results of best fits using least-squares method for comparison with the MCMC statistical analyses. Here we used the *NonlinearModelFit* command of *Wolfram Mathematica*.

**Table A1** – The parameters of the best-fit model for galaxy U5750

| Profiles | $\rho_0 \pm \sigma_{\rho_0}$, $\left(10^{-3}\frac{M_\odot}{pc^3}\right)$ | $r_0 \pm \sigma_{r_0}$, (kpc) | $r_{vir}$, (kpc) | $M_{vir}$, $(10^{10}M_\odot)$ | $M \pm \sigma_M{}^a$, $(10^{10}M_\odot)$ | $M \pm \sigma_M{}^b$, $(10^9 M_\odot)$ | $\Delta$BIC | $\chi^2$ |
|---|---|---|---|---|---|---|---|---|
| Beta | $9.15 \pm 0.28$ | $6.85 \pm 0.21$ | 46.97 | 6.04 | $3.40 \pm 0.23$ | $6.44 \pm 0.84$ | 26.08 | 0.28 |
| Brown. | $7.56 \pm 0.06$ | $6.47 \pm 0.05$ | 42.04 | 4.83 | $3.15 \pm 0.06$ | $5.96 \pm 0.22$ | 0 | 0.03 |
| Burkert | $11.73 \pm 0.65$ | $7.16 \pm 0.38$ | 51.26 | 7.16 | $3.54 \pm 0.42$ | $6.88 \pm 1.61$ | 34.18 | 0.70 |
| Exp. sph. | $12.50 \pm 0.50$ | $5.11 \pm 0.19$ | 31.26 | 3.95 | $3.34 \pm 0.32$ | $3.36 \pm 0.55$ | 29.91 | 0.47 |
| ISO | $10.70 \pm 1.00$ | $4.23 \pm 0.38$ | 83.43 | 18.57 | $3.85 \pm 0.69$ | $2.19 \pm 0.87$ | 41.57 | 1.37 |
| Persic | — | — | — | — | 3.44 | — | 33.13 | 0.64 |

For the Persic profile $\beta_0 = 88.31 \pm 2.63$, and $a = 6.73 \pm 0.35$.

For galaxy U5750, the BIC value is minimal for the Brownstein profile and maximal for the ISO profile, as shown in Table 1.

The values BIC = {49.36, 43.53, 19.45, 61.02, 52.58, 53.63} are for the Exp. sph., Beta, Brownstein, ISO and Persic, and Burkert. The $\text{BIC}_0 = 19.45$ is for the Brownstein profile.

**Table A2** – The parameters of the best-fit model for galaxy U11454

| Profiles | $\rho_0 \pm \sigma_{\rho_0}$, $\left(10^{-3}\frac{M_\odot}{pc^3}\right)$ | $r_0 \pm \sigma_{r_0}$, (kpc) | $r_{vir}$, (kpc) | $M_{vir}$, $(10^{11}M_\odot)$ | $M \pm \sigma_M{}^a$, $(10^{10}M_\odot)$ | $M \pm \sigma_M{}^b$, $(10^{10}M_\odot)$ | $\Delta$BIC | $\chi^2$ |
|---|---|---|---|---|---|---|---|---|
| Beta | $103.97 \pm 10.79$ | $3.65 \pm 0.23$ | 56.82 | 1.56 | $6.00 \pm 1.00$ | $1.11 \pm 0.32$ | 16.24 | 14.79 |
| Brown. | $80.56 \pm 10.10$ | $3.62 \pm 0.26$ | 51.73 | 1.27 | $5.75 \pm 1.17$ | $1.10 \pm 0.37$ | 23.96 | 28.14 |
| Burkert | $139.04 \pm 12.88$ | $3.70 \pm 0.21$ | 62.30 | 1.86 | $6.14 \pm 0.91$ | $1.13 \pm 0.30$ | 11.31 | 9.81 |
| Exp. sph. | $130.87 \pm 12.86$ | $2.84 \pm 0.17$ | 24.07 | 0.75 | $5.95 \pm 0.99$ | $0.61 \pm 0.16$ | 17.83 | 16.89 |
| ISO | $151.21 \pm 11.74$ | $1.93 \pm 0.10$ | 142.80 | 9.86 | $6.47 \pm 0.77$ | $0.30 \pm 0.07$ | 0 | 3.82 |
| Persic | — | — | — | — | 5.95 | — | 8.97 | 8.07 |

For the Persic profile $\beta_0 = 155.85 \pm 2.63$, and $a = 3.33 \pm 0.20$.

The values BIC = {76.51, 83.78, 78.85, 85.37, 67.54, 91.50} are for the Persic, Beta, Burkert, Exp. sph., ISO, and Brownstein. Here, $\text{BIC}_0 = 67.54$ is for the ISO. However, there is not a significant difference between the values BIC (see Table A2). Additionally, the value of $\chi^2$ is greatest for the Brownstein profile and smallest for the ISO. It should be mentioned that the results obtained using the MCMC method (Table 2) do not differ significantly from the results obtained by the fitting method.

**Table A3** – The parameters of the best-fit model for galaxy U11648

| Profiles | $\rho_0 \pm \sigma_{\rho_0}$, $\left(10^{-3}\frac{M_\odot}{pc^3}\right)$ | $r_0 \pm \sigma_{r_0}$, (kpc) | $r_{vir}$, (kpc) | $M_{vir}$, $(10^{11}M_\odot)$ | $M \pm \sigma_M{}^a$, $(10^{10}M_\odot)$ | $M \pm \sigma_M{}^b$, $(10^9 M_\odot)$ | $\Delta$BIC | $\chi^2$ |
|---|---|---|---|---|---|---|---|---|
| Beta | $60.95\pm10.54$ | $4.17\pm0.45$ | 54.19 | 1.26 | $4.90\pm1.38$ | $9.67\pm4.78$ | 12.59 | 132.56 |
| Brown. | $45.90\pm7.96$ | $4.20\pm0.44$ | 49.76 | 1.05 | $4.77\pm1.36$ | $9.85\pm4.74$ | 18.98 | 177.22 |
| Burkert | $81.87\pm14.09$ | $4.22\pm0.47$ | 59.19 | 1.49 | $4.99\pm1.38$ | $9.81\pm4.91$ | 8.29 | 108.99 |
| Exp. sph. | $73.82\pm11.34$ | $3.33\pm0.32$ | 26.33 | 0.68 | $5.04\pm1.31$ | $5.53\pm2.43$ | 11.31 | 125.05 |
| ISO | $105.98\pm20.70$ | $1.95\pm0.25$ | 120.86 | 5.95 | $5.02\pm1.50$ | $2.11\pm1.22$ | 0 | 74.78 |
| Persic | – | – | – | – | 4.68 | – | 7.76 | 106.41 |

For the Persic profile $\beta_0 = 133.72 \pm 5.03$, and $a = 3.55 \pm 0.43$.

The values BIC = {182.38, 174.09, 186.68, 185.40, 193.07, 181.85} are for the Burkert, ISO, Beta, Exp. sph., Brownstein, and Persic. Here, $\mathrm{BIC}_0 = 174.09$ is for the ISO.

**Table A4** – The parameters of the best-fit model for galaxy U11819

| Profiles | $\rho_0 \pm \sigma_{\rho_0}$, $\left(10^{-3}\frac{M_\odot}{pc^3}\right)$ | $r_0 \pm \sigma_{r_0}$, (kpc) | $r_{vir}$, (kpc) | $M_{vir}$, $(10^{11}M_\odot)$ | $M \pm \sigma_M{}^a$, $(10^{10}M_\odot)$ | $M \pm \sigma_M{}^b$, $(10^{10}M_\odot)$ | $\Delta$BIC | $\chi^2$ |
|---|---|---|---|---|---|---|---|---|
| Beta | $76.35\pm2.54$ | $4.61\pm0.12$ | 64.66 | 2.20 | $6.88\pm0.41$ | $1.64\pm0.19$ | 4.39 | 2.21 |
| Brown. | $62.14\pm2.17$ | $4.35\pm0.11$ | 57.11 | 1.66 | $6.48\pm0.42$ | $1.49\pm0.17$ | 11.06 | 3.45 |
| Burkert | $98.32\pm3.88$ | $4.84\pm0.15$ | 72.35 | 2.79 | $7.07\pm0.49$ | $1.78\pm0.25$ | 5.96 | 2.45 |
| Exp. sph. | $107.35\pm3.19$ | $3.32\pm0.08$ | 27.50 | 0.98 | $6.77\pm0.38$ | $0.80\pm0.08$ | 13.7 | 1.65 |
| ISO | $88.92\pm5.29$ | $2.93\pm0.15$ | 166.70 | 15.58 | $7.51\pm0.74$ | $0.60\pm0.13$ | 0 | 4.11 |
| Persic | – | – | – | – | 6.84 | – | 7.9 | 2.79 |

Notice that for the Persic profile $\beta_0 = 174.44 \pm 2.59$, and $a = 4.62 \pm 0.15$.

The values BIC = {92.63, 83.32, 84.89, 78.93, 86.83, 89.99} are for the Exp. sph., Beta, Burkert, ISO, Persic, and Brownstein. Here, $\mathrm{BIC}_0 = 78.93$ is for ISO.

**References**

1 Bertone G., Hooper D. and Silk J. Particle dark matter: evidence, candidates and constraints // Physics Reports. – 2005. – Vol. 405. – P. 279-309. https://doi.org/10.1016/j.physrep.2004.08.031

2 Dodelson S. Modern Cosmology//Academic Press. – 2010. – p. 456.

3 Planck Collaboration, Ade P.A.R. e.a.P.C. Planck 2013 results. I. Overview of products and scientific results // Astronomy and Astrophysics. – 2014. – Vol. 571. – A1. https://doi.org/10.1051/0004-6361/201321529

4 Horace W. Babcock The rotation of the Andromeda Nebula // Lick Observatory Bulletin. – 1939. – Vol. 498. – P. 41-51. 10.5479/ADS/b/1939LicOB.19.41B

5 van de Hulst H.C., Raimond E. and van Woerden H. Rotation and density distribution of the Andromeda nebula derived from observations of the 21-cm line // Bulletin of the Astronomical Institutes of the Netherlands. – 1957. – Vol. 14. – p.1.

6 Volders L.M. Neutral hydrogen in M 33 and M 101 // Bulletin of the Astronomical Institutes of the Netherlands. – 1959. – Vol. 14. – p. 343.

7. de Blok W.J.G., McGaugh S.S. and Rubin V.C. High-resolution rotation curves of low surface brightness galaxies. II. Mass models // The Astronomical Journal. – 2001. – Vol. 122. – P. 2396-2427. https://doi.org/10.1086/323450

8. McGaugh S.S., Rubin V.C. and De Blok W.J.G. High-resolution rotation curves of low surface brightness galaxies. I. Data // The Astronomical Journal. – 2001. – Vol. 122. – P. 2381-2395. https://doi.org/10.1086/323448

9 de Blok W.J.G. and Bosma A. High-resolution rotation curves of low surface brightness galaxies // Astronomy and Astrophysics. – 2002. – Vol. 385. – P. 816-846. https://doi.org/10.1051/0004-6361:20020080

10 Barranco J., Bernal A. and Nunez D. Dark matter equation of state from rotational curves of galaxies // Monthly Notices of the Royal Astronomical Society. – 2015 – Vol. 449. – P. 403-413. https://doi.org/10.1093/mnras/stv302

11 de Blok W.J.G. and McGaugh S.S. Does low surface brightness mean low density? // The Astrophysical Journal. –1996. – Vol. 469. – P. 89-92. https://doi.org/10.1086/310266

12 de Blok W.J.G. and McGaugh S.S. The dark and visible matter content of low surface brightness disc galaxies // Monthly Notices of the Royal Astronomical Society. – 1997. – Vol. 290. – P. 533-552. https://doi.org/10.1093/mnras/290.3.533

13 Blais-Ouellette S., Amram P. and Carignan C. Accurate Determination of the Mass Distribution in Spiral Galaxies. II. Testing the Shape of Dark Halos // The Astronomical Journal. – 2001. – Vol. 121. – P.1952-1964. https://doi.org/10.1086/319944

14 Burkert A. The structure of dark matter halos in dwarf galaxies // The Astrophysical Journal Letters. – 1995 – Vol. 447. – P. 25-28. https://doi.org/10.1086/309560

15 Jimenez R., Verde L., Oh S.P. Dark halo properties from rotation curves // Monthly Notices of the Royal Astronomical Society. – 2003 – Vol. 339. – P. 243-259. https://doi.org/10.1046/j.1365-8711.2003.06165.x

16 Sofue Y. Rotation curve of the Milky Way and the dark matter density // Galaxies. – 2020 – Vol. 8. – P. 37. https://doi.org/10.3390/galaxies8020037

17 Brownstein J.R. and Moffat J.W. Galaxy rotation curves without nonbaryonic dark matter // The Astrophysical Journal. – 2006. – Vol. 636. – P. 721-741. https://doi.org/10.1086/498208

18 Navarro J.F., Frenk C.S., White S.D.M. Simulations of X-ray clusters // Monthly Notices of the Royal Astronomical Society. – 1995 – Vol. 275. – P. 720-740. https://doi.org/10.1093/mnras/275.3.720

19 Persic M., Salucci P. and Stel F. The universal rotation curve of spiral galaxies – I. The dark matter connection. // Monthly Notices of the Royal Astronomical Society. – 1996. – Vol. 281. – P. 27-47. https://doi.org/10.1093/mnras/278.1.27

20 Sofue Y. Rotation curve and mass distribution in the galactic center – From Black hole to entire galaxy // Publications of the Astronomical Society of Japan. – 2013 – Vol. 65. – P. 118. https://doi.org/10.1093/pasj/65.6.118

21 Levenberg K. A method for the solution of certain non-linear problems in least squares // Quarterly of Applied Mathematics. – 1944. – Vol. 2. – P. 164-168. https://doi.org/10.1090/qam/10666

22 Marquardt D. An algorithm for least-squares estimation of nonlinear parameters // Journal on applied mathematics. – 1963. – Vol. 11. – P. 431-441. https://doi.org/10.1137/0111030

23 Schwarz G. D. Estimating the Dimension of a Model // Annals of Statistics. – 1963. – Vol. 6. – P. 461-464. 10.1214/aos/1176344136

24 Siutsou I., Argüelles C.R. and Ruffini R. Dark matter massive fermions and Einasto profiles in galactic haloes // Astronomy Reports. – 2015 – Vol. 59. – P. 656-666. https://doi.org/10.1134/S1063772915070124

25 Arjona R., Cardona W. and Nesseris S. Unraveling the effective fluid approach for f (R) models in the subhorizon approximation // Physical Review D. – 2019. – Vol. 99. – P. 043516. https://doi.org/10.1103/PhysRevD.99.043516

26 Boshkayev K., Konysbayev T., Kurmanov E. and Muccino M. Dark matter properties in galaxy U5750 // News of the National Academy of Sciences of the Republic of Kazakhstan physico-mathematical series. – 2020. – Vol. 6. – P.81-90. https://doi.org/10.32014/2020.2518-1726.101

27 Boshkayev K., Konysbayev T., Kurmanov E., Muccino M. and Zhumakhanova G. Physical properties of dark matter in galaxy U11454 // Physical sciences and technology. – 2020. – Vol. 7. – P.11-20. https://doi.org/10.26577/phst.2020.v7.i2.02

28 Boshkayev K., Konysbayev T., Kurmanov E., Luongo O., Muccino M. Imprint of pressure on characteristic dark matter profiles: the case of ESO0140040 // Galaxies. – 2020. – Vol.74. – P.1-13. https://doi.org/10.3390/galaxies8040074

39 Bernal T. et al. Rotation curves of high-resolution LSB and SPARC galaxies with fuzzy and multistate (ultralight boson) scalar field dark matter //Monthly Notices of the Royal Astronomical Society. – 2018. – V. 475. – P. 1447-1468. https://doi.org/10.1093/mnras/stx3208

30 Duangchan Ch., Sinpaiboon W., Chantaso N., Haethaisong W., Wechakama M. Effect comparison of dark matter annihilation pressure to NFW and pseudo-isothermal profiles of low surface brightness galaxies // J. Phys.: Conf. Ser. – 2020. – Vol. 1719. – P. 012014. https://doi.org/10.1088/1742-6596/1719/1/012014

31 Boshkayev K., Konysbayev T., Kurmanov Ye., Luongo O. and Malafarina D. Accretion Disk Luminosity for Black Holes Surrounded by Dark Matter with Tangential Pressure // The Astrophysical Journal. – 2022. – Vol. 936. – P. 1-7. https://doi.org/10.3847/1538-4357/ac8804

32 Kurmanov E., Boshkayev K., Giambo R., Konysbayev T., Luongo O., Malafarina D. and Quevedo H. Accretion disk luminosity for black holes surrounded by dark matter with anisotropic pressure // The Astrophysical Journal. – 2022. – Vol. 925. – P. 1-8. https://doi.org/10.3847/1538-4357/ac41d4

33. Boshkayev K., Idrissov A., Luongo O. and Malafarina D. Accretion disc luminosity for black holes surrounded by dark matter // Monthly Notices of the Royal Astronomical Society. – 2020. – Vol. 496. – P. 1115-1123. https://doi.org/10.1093/mnras/staa1564

34 Boshkayev K., Konysbayev T., Kurmanov E., Luongo O., Malafarina D., Mutalipova K. and Zhumakhanova G. Effects of non-vanishing dark matter pressure in the Milky Way galaxy // Monthly Notices of the Royal Astronomical Society. – 2021. – Vol. 508. – P. 1543-1554. https://doi.org/10.1093/mnras/stab2571

35 Boshkayev K. Konysbayev T., Kurmanov E., Luongo O., Muccino M., Quevedo H., Taukenova A. and Zhumakhanova G. Motion of stars near the galactic center // International Journal of Mathematics and Physics. – 2021. – Vol. 12. – P. 79-86. https://doi.org/10.26577/ijmph.2021.v12.i2.09

36 Boshkayev K., Zhumakhanova G., Mutalipova K., Muccino M. Investigation of different dark matter profiles // News of the National Academy of Sciences of the Republic of Kazakhstan Physical and Mathematical Series. Volume 6, number 328 (2019), 25 – 33. https://doi.org/10.32014/2019.2518-1726.70

37 Di Paolo C., Salucci P. and Erkurt A. The universal rotation curve of low surface between galaxies – IV. The interrelation between dark and luminous matter // Monthly Notices of the Royal Astronomical Society. – 2019. – Vol. 490. – P. 5451-5477. https://doi.org/10.1093/mnras/stz2700

38 Sofue Y., Dark halos of M 31 and the Milky Way // Publications of the Astronomical Society of Japan.- 2015.- Vol. 67.- P. 75. https://doi.org/10.1093/pasj/psv042

39 Sofue Y., Rotation and mass in the Milky Way and spiral galaxies // Publications of the Astronomical Society of Japan.- 2017. – Vol. 69. –P. R1. https://doi.org/10.1093/pasj/psw103

40 de Lavallaz A., Fairbairn M. Neutron stars as dark matter probes // Physical Review D. -2010. – Vol. 81. – Issue 12. – id. 123521. https://doi.org/10.1103/PhysRevD.81.123521

41 Zheng H., Sun K-J., Chen L.-W. Old Neutron Stars as Probes of Isospin-Violating Dark Matter // The Astrophysical Journal. – 2015. – Vol. 800. – Issue 2. – article id. 141. https://doi.org/10.1088/0004-637X/800/2/141

42 Ruffini R., Arguelles C. R., Rueda J. A., On the core-halo distribution of dark matter in galaxies // Monthly Notices of the Royal Astronomical Society.- 2015.-Vol. 451.- P. 622. https://doi.org/10.1093/mnras/stv1016

43 Arguelles C. R., Krut A., Rueda J. A., Ruffini R., Novel constraints on fermionic dark matter from galactic observables I: The Milky Way // Physics of the Dark Universe.-2018.-Vol. 21. – P. 82. https://doi.org/10.1016/j.dark.2018.07.002

44 Arguelles C. R., Krut A., Rueda J. A., Ruffini R., Novel constraints on fermionic dark matter from galactic observables II: Galaxy scaling relations // Physics of the Dark Universe.-2019.- Vol. 24.-P. 100278. https://doi.org/10.1016/j.dark.2019.100278

45 Argüelles C.R., Boshkayev K., Krut A., Nurbakhyt G., Rueda J.A., Ruffini R., Uribe-Suárez J.D., Yunis R. On the growth of supermassive black holes formed from the gravitational collapse of fermionic dark matter cores // Monthly Notices of the Royal Astronomical Society.- 2023.-Vol. 523.- Issue 2.- P.2209-2218. https://doi.org/10.1093/mnras/stad1380

46 Guzmán F. S., Matos T. Scalar fields as dark matter in spiral galaxies //Classical and Quantum Gravity. – 2000. – Volume. 17. – №. 1. – P. L9. https://doi.org/10.1088/0264-9381/17/1/102

47 Boehmer C. G., Harko T. Can dark matter be a Bose–Einstein condensate? //Journal of Cosmology and Astroparticle Physics. – 2007. – Volume. 2007. – №. 06. – P. 025. https://doi.org/10.1088/1475-7516/2007/06/025

48 Robles V. H., Matos T. Exact solution to finite temperature SFDM: natural cores without feedback //The Astrophysical Journal. – 2012. – Volume. 763. – №. 1. – P. 19. https://doi.org/10.1088/0004-637X/763/1/19

49 Lubini M., Tortora C., Näf J., Jetzer Ph., Capozziello S. Probing the dark matter issue in f(R)-gravity via gravitational lensing // The European Physical Journal C. – 2011. – Vol.71. – article id. 1834. https://doi.org/10.1140/epjc/s10052-011-1834-8

50 Capozziello S., Cardone V.F., Troisi A. Low surface brightness galaxy rotation curves in the low energy limit of Rn gravity: no need for dark matter? // Monthly Notices of the Royal Astronomical Society. – 2007. – Vol. – 375. – Issue 4. – P. 1423-1440. https://doi.org/10.1111/j.1365-2966.2007.11401.x